# Interpretation of Simultaneous Mechanical-Electrical-Thermal Failure in a Lithium-Ion Battery Module

## Preprint

Chao Zhang, Shriram Santhanagopalan,
Mark J. Stock, Nicholas Brunhart-Lupo,
and Kenny Gruchalla
*National Renewable Energy Laboratory*

**NOTICE**

This report is available at no cost from the National Renewable Energy Laboratory (NREL) at www.nrel.gov/publications.

Available electronically at SciTech Connect http:/www.osti.gov/scitech

Available for a processing fee to U.S. Department of Energy and its contractors, in paper, from:

> U.S. Department of Energy
> Office of Scientific and Technical Information
> P.O. Box 62
> Oak Ridge, TN 37831-0062
> OSTI http://www.osti.gov
> Phone: 865.576.8401
> Fax: 865.576.5728
> Email: reports@osti.gov

Available for sale to the public, in paper, from:

> U.S. Department of Commerce
> National Technical Information Service
> 5301 Shawnee Road
> Alexandria, VA 22312
> NTIS http://www.ntis.gov
> Phone: 800.553.6847 or 703.605.6000
> Fax: 703.605.6900
> Email: orders@ntis.gov

*Cover Photos by Dennis Schroeder: (left to right) NREL 26173, NREL 18302, NREL 19758, NREL 29642, NREL 19795.*

NREL prints on paper that contains recycled content.

# Interpretation of Simultaneous Mechanical-Electrical-Thermal Failure in a Lithium-Ion Battery Module

Chao Zhang[1], Shriram Santhanagopalan[2], Mark J. Stock[1], Nicholas Brunhart-Lupo[1], Kenny Gruchalla[1]
*[1]Computational Science Center*
*[2]Transportation and Hydrogen Systems Center*
*National Renewable Energy Laboratory*
*Golden, CO*
*chao.zhang@nrel.gov, shriram.santhanagopalan@nrel.gov, mark.stock@nrel.gov,*
*nicholas.brunhart-lupo@nrel.gov, kenny.gruchalla@nrel.gov*

*Abstract*—**Lithium-ion batteries are currently the state-of-the-art power sources for electric vehicles, and their safety behavior when subjected to abuse, such as a mechanical impact, is of critical concern. A coupled mechanical-electrical-thermal model for simulating the behavior of a lithium-ion battery under a mechanical crush has been developed. We present a series of production-quality visualizations to illustrate the complex mechanical and electrical interactions in this model.**

*Keywords—Lithium Battery, Mechanical Impact, Short Circuit*

## 1. Introduction

The safety behavior of lithium-ion batteries (LIBs) subjected to an external mechanical crush is a critical concern when employing these batteries in electrical vehicle applications. The physical phenomena occurring in LIBs are very complicated and take place in different time and length scales (particle, electrode, cell and pack), including electro-chemical reactions at the porous active materials, electrons moving across current collectors, heat generation due to charge/discharge, chemical reactions at the interface between the electrolyte and the electrode, mechanical deformation under external crush, and most importantly, the coupling effect among these multi-physics responses. Computational models are an ideal way to study interactions across these multiple domains and provide insights to the design of safer LIBs.

Recently, we presented the first coupled mechanical-electrical-thermal model for simulating short circuits induced by a mechanical crush and identified the interaction of mechanical failure and consequential electrical-thermal response [1,2]. A simultaneous coupling approach on a representative sandwich (RS) was developed, which predicts the simultaneous evolution of electrical and thermal responses associated with mechanical deformation for a single battery cell [2].

Previous models reported in the literature focus exclusively on the mechanical response at the cell-level [3-6]. Comparatively fewer studies have examined module-level or larger battery hardware, which involves thermal propagation following the formation of internal short circuits [7]. Recently, Marcicki et al. [7] presented a new method for measuring fault currents and described a more complete picture of module-level failure during an abusive crush. In this work, we extend our approach for modeling the mechanical-electrical failure behavior of a lithium-ion battery module, which contains 20 battery cells connected in parallel. While the evaluation of mechanical failure is straightforward and can be quantified using the stress/strain response or other failure parameters, the initiation of short circuit involves a significant change in the electrical current (an increase of $10^3$~$10^5$ times) and a continuous change in the electrical conductivity of the different cell components over 2-3 orders of magnitude during the propagation of short circuit.

The differences in the species flux due to the differences in material properties on either side of the interface and an exponential dependence of the reaction rates on the local over potential further limit the interpretation of the results. For instance, identification of the onset location of short circuit involves isolation of the elements across the interface where the mechanical failure threshold has been met, followed by identification of the local electrical resistance of the individual components at the interface. The process will be further complicated with the introduction of multiple cells connected in parallel within one module. In this case the propagation of electrical short circuit current resulting from mechanical failure across different battery cells and the combined effect of short circuit locations distributed across multiple cells are too complicated to interpret using traditional tools available for data processing. To help tease apart this complexity, a series of production-quality visualizations were produced to illustrate different aspects of the simulation.

## 2. Modeling & Simulation

The lithium-ion battery studied in this work is comprised of 15 Ah pouch cells with a nominal voltage of 3.65 V, and is fully charged to 4.15 V prior to each test. The pouch cells have an in-plane dimension of 226 mm x 164 mm and a thickness of 5.4 mm. Each cell contains 16 cathode layers and 17 anode layers, stacked periodically and electrically isolated by polymeric separator layers. Each of these layers range in thickness from 8 μm to 120 μm. Modeling the individual layers is computationally costly. However, predicting a short circuit involves modeling local damage across each of the individual components (separators, collectors and active materials).
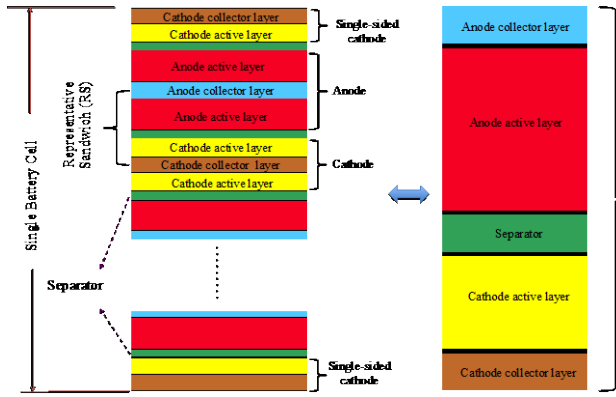
1

Figure 1: Cross-sectional view of a pouch cell and schematic of a representative sandwich (RS): the pouch cell is represented by a single RS which represents the proportional thickness of each individual battery component.

In this work, we employ a representative sandwich (RS) model (shown in Figures 1 and 2) which we previously developed [2] to explicitly model each individual component without loss of computational efficiency or accuracy.

## 2.1 Coupled mechanical-electrical model

The coupled mechanical-electrical model is built in the commercial finite element software LS-DYNA [8] using modules available by default: solid mechanics solver and electromagnetic (EM) solver. The basic equations for these two solvers are listed below. The mechanical solver is used to solve for deformation and predict failure of a structure suffering external or internal loading conditions. The explicit mechanical solver seeks a solution to the momentum conservation equation

$$\sigma_{ij,j} + \rho f_i = \rho u_{i,tt} \tag{1}$$

where $\sigma_{ij}$ denotes components of stress, $u_i$ denotes components of displacement, $\rho$ is the density, $f_i$ is the body force density and $t$ is time. The subscript on $\sigma_{ij,j}$ denotes covariant differentiation, similarly, $u_{i,tt}$ denotes acceleration.

The LS-DYNA EM solver employs the eddy current approximation [9] which assumes a divergence free current density and no charge accumulation. Two equations constituting the system response are solved:

$$\nabla(\kappa \vec{\nabla} \varphi) = 0 \tag{2}$$

$$\kappa \frac{\partial \vec{A}}{\partial t} + \vec{\nabla} \times (\frac{1}{\mu} \vec{\nabla} \times \vec{A}) + \kappa \vec{\nabla} \varphi = \vec{j}_s \tag{3}$$

where magnetic vector potential $\vec{A}$ and electric scalar potential $\phi$ are two unknowns to be solved; $\kappa$ is the electrical conductivity, $\mu$ is the magnetic permeability and $\vec{j}_s$ is the source current density. In LS-DYNA, the mechanical and EM solvers are fully coupled with each other. Details of the coupling methodology were presented earlier [2]. The two

solvers have distinct time steps, and generally the mechanical time step is a lot smaller than the EM time step, in keeping with the time constants for the relevant physics. At each mechanical time step, the EM field values are calculated by linear interpolation.



Figure 2: 3D expanded view of several of the battery module's layers and components.

## 2.2 Mechanical-electrical failure

The objective of this work is to predict the structural fracture-induced electrical short-circuit of a lithium-ion battery under an external impact load. Proper failure criteria and failure parameters should be implemented and defined to enable this capability.

In this work, a maximum tensile failure criterion was implemented and the Honeycomb Material Model in LS-DYNA was utilized to simulate separator failure. The tensile failure strain is determined as 0.29 based on previous parametric studies on the failure of a single battery cell subjected to indentation [2]. The electrical contact is defined using a distance-based criterion, which implies that electrical contact between two parts initiates when the distance between them is below a certain threshold value $d_c$. This threshold value is set to 0.039 mm based on our earlier work [2].
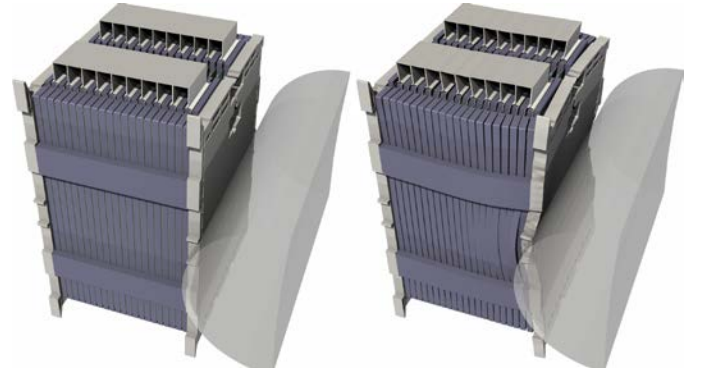


Figure 3: ParaView OSPRay rendered view of the external geometry of the battery model with impactor for a 20-cell lithium-ion battery module (left: before impact, right: after impact).
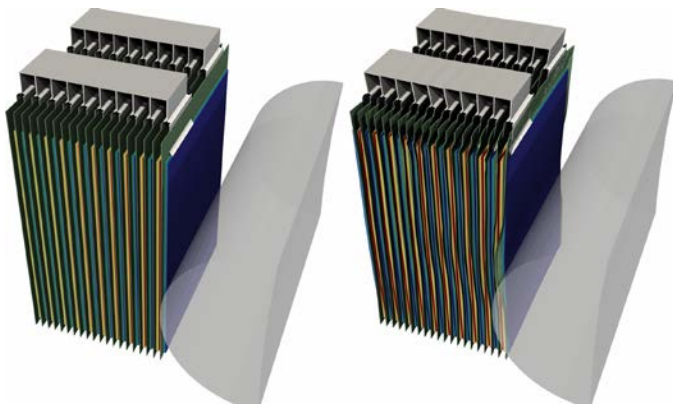
2

Figure 4: ParaView OSPRay rendered view of the internal geometry of the battery model with impactor for a 20-cell lithium-ion battery module (left: before impact, right: after impact).

## 2.3 Numerical implementation

Twenty battery cells are connected in parallel using a bus bar. Once short circuit initiates within one of these cells, current from the other cells flows across the bus bar discharging multiple cells across the short circuit resistance, resulting in propagation of the thermal and electrical failure. Each battery cell model was meshed using solid elements, with 2 elements through the thickness ($z$-direction) of each layer, 50 elements along the length ($x$-direction) and 50 elements through the width ($y$-direction) resulting a total of 25000 elements per cell for the RS model. The external frames and panels of the battery module are meshed with an average element size of 3 mm. The impactor is a cylindrical platen of 150 mm diameter, and is modeled as a rigid cylinder. There are a total of 745,304 elements in the finite element model.

For the impact simulation, an initial velocity 6.3 m/s, corresponding to a drop velocity from 2 m height, is assigned to the impactor. Figures 3 and 4 show the external and internal geometries before and after the impact. The degrees of freedom for the back panel are fixed to represent the constraints on the battery module. Contacts are defined between every two sets of components to avoid deformation-induced penetration. The porous active materials and separator are treated as homogeneous solid materials. The current collectors, tabs, bus bar, external frames, and panels are modeled using a computational representation exhibiting isotropic-hardening plasticity. The electrical properties of all components are considered to be isotropic. All input parameters are listed in [2].

The numerical model was solved on the High Performance Computing system, Peregrine [10] at the National Renewable Energy Laboratory (NREL). The time step for the mechanical part is $1 \times 10^{-8}$ s, and that for the EM part is $1 \times 10^{-5}$ s. The computational time to simulate 3 ms of the impact test is about 34 hours using 60 large-memory (256 GB) 16-core nodes.

## 3. Visualization

The comprensive visualization of these data is a challenging problem. The coupling of mechanical, electrical, and thermal physical phenomena produce a highly multivariate collection of data on a variety of components, many of which are encapsulated or otherwise occluded by other components. Futhermore, the electrical conductivity of different components can vary by orders of magnitude. For example, the conductivity across the cathode active material is as low as 100 S/m, whereas that across the tabs is 1e7 S/m. The vast differences in thickness of the different components (from a few microns to several inches) only compound the interpretation of the flux evolution. As a result, during mechanical crush, the current density reaches 300 A/m$^2$ on the surface the active anode and cathode at the location of the short circuits, but at the same time the current density exceeds 25,000 A/m$^2$ on the battery tabs. To help tease apart these complex interactions, a series of production-quality visualizations were produced to illustrate different aspects of the simulation, isolating components with similar electrical conductivty and taking a variety of exploded and clipped views.

The production-quality visualizations were rendered in Blender [11] and ParaView [12], with geometry and simulation data exported using LS-PrePost. LS-PrePost, the pre- and post-processor from LSTC, was used primarily to process the binary LS-DYNA output into formats that ParaView could read in bulk. Custom Perl scripts generated macro files, which were processed by LS-PrePlot in batch. The exterior and interior geometry animations were generated from sets of STL files: one for each of 12 parts at each of 152 time steps. ParaView read the set of 1824 STL files, and was able to export animations using OSPRay rendering. OSPRay is a CPU only raytracer built on top of Intel's Embree [13], which provides superscalar-accelerated CPU raytracing kernels. Our 16-core workstations took 2-15 seconds to create each frame at Full HD resolution with multiple ambient rays and multiple rays per pixel.

Visualizing the direction and magnitude of the local electric current densities across the different components of the battery module is the most tangible approach to studying failure propagation within the module. To visualize the data field on components, we used LS-PrePlot macro files to set up the variables, elements, and ranges, and then write a VRML2 file with color information for each time step. These files were converted to PLY format via command-line MeshLab (meshlabserver) [14], which retains the color information. Each frame in these clips was rendered from a ParaView Python script using pvbatch. In this script, the PLY file is read, several filters applied, including the Calculator filter to convert the color value back into a scalar or vector, and ultimately visualized as a color texture or 3D vector glyphs using ParaView's built-in OSPRay renderer.

The current density distribution on the surface of the active anodes and cathodes in the plane of the mechanical crush was of particular interest, as this was a direct representation of internal short circuits. To visualize the in-plane current density on the surface of the anodes and cathodes, we produced an illumination-based visualization using Blender's Cycles rendering system with a surface light emission shader (see Figure 5). We once again used the exported VMRL2 geometry from LS-PrePlot, which provided the shells of the simulation meshes with the $x$-component of current density encoded into the vertex color of that geometry.

3

Figure 5: Blender rendered exploded view of the in-plane current density distribution on the surface of the active anode and cathode, illustrating the locations of the short circuit.

The color of the emitted light was provided by simulated blackbody radiation; the current density was mapped to the range of 0 to 14,000° K, which gives a strong blue-white hue at the maximum. The strength of this emission was also controlled by current density, $c$. By normalizing the density into the range $[0,1]$ (that is, the absolute value of the current density as divided by its maximum), the irradiance (W/m$^2$) is given as the quantity $(c + 1)^5$. To marginalize regions that do not experience high current density, we use the normalized current density to mediate (by linear mix) between this emission shader and a translucent bidirectional scattering distribution function. Frames were rendered on a visualization server equipped with 3 Nvidia K6000 GPUs, using 576 samples per pixel.

## 4. Discussion

In the absence of an external electrical load across the busbar, there should be no internal in-plane current. However, during an external crush one or more of the internal cell components reaches or exceeds the mechanical failure criteria resulting in a drop in electrical resistance and initiation of alternate pathways for the electric current to flow from the positive to the negative electrodes. Of these numerous pathways, the evolution of an electrical short-circuit across specific sets of components, is determined by the physical proximity between the energized layers, the rate of decrease of electrical resistance in the layer across as well as the existence of conduction pathways far away from the local element subjected to mechanical failure. The simultaneous visualization of multiple physical variables of interest, such as the components of the von Mises stress together with the local current density distribution enabled accurate determination not only the location where mechanical failure or short-circuit originates, but also the mechanism of failure propagation. For instance, on Figures 3 and 4, we see that the structural integrity provided by the end-plates significantly reduces the mechanical impact on the cells' internal components; however, from Figure 5, it is obvious that electrical short-circuits happening in the cells farthest from the impactor are primarily due to the mechanical resistance of the end-plates located right next to these cells.

Without a simultaneous visualization of the entire module's multi-physics response, it would have been impossible to track the propagation of a secondary set of failure events that originate from the rear end of the module, as a result of packaging. Such results have far-reaching implications for design of battery packs – in this example, one would consider the mechanical properties of packaging between the end-plates and the cells, in addition to the separation between individual cells.

### REFERENCES

[1] C. Zhang, S. Santhanagopalan, M. A. Sprague and A. A. Pesaran, "Coupled mechanical-electrical-thermal modeling for short-circuit prediction in a lithium-Ion cell under mechanical abuse," J. Power Sources, vol. 290, pp. 102–113, 2015.

[2] C. Zhang, S. Santhanagopalan, M. A. Sprague and A. A. Pesaran, "A representative sandwich model for coupled mechanical-electrical-thermal simulation of lithium-ion battery under quasi-static indentation tests," J. Power Sources, vol. 298, pp. 309–321, 2015.

[3] L. Greve and C. Fehrenbach, "Mechanical testing and macro-mechanical finite element smulation of the deformation, fracture, and short circuit initiation of cylindrical lithium ion battery cells," J. Power Sources, vol. 214, pp. 377–385, 2014.

[4] J. Lamb and C. J. Orendorff, "Evaluation of mechanical abuse techniques in lithium ion batteries," J. Power Sources, vol. 247, pp. 189–196, 2014.

[5] W. J. Lai, M. Y. Ali and J. Pan, "Mechanical behavior of representative volume elements of lithium-ion battery modules under various loading conditions," J. Power Sources, vol. 248, pp. 789–808, 2014.

[6] Y. Xia, T. Li, F. Ren, Y. Gao and H. Wang, "Failure analysis of pinch-torsion tests as a thermal runaway risk evaluation method of Li-ion cells," J. Power Sources, vol. 265, pp. 356–362, 2014.

[7] J. Marcicki, X. G. Yang and P. Rairigh, "Fault current measurements during cursh testing of electrically parallel lithium-ion battery modules," ECS Electrochem. Lett., vol. 9, pp. A97-A99, 2015.

[8] J. O. Hallquist, LS-DYNA Keyword User's Manual. Livermore Software Technology Corporation, 970, 2007.

[9] A. A. Rodriguez and A. Valli, Eddy Current Approximation of Maxwell Equations: Theory, Algorithms and Applications. Springer Science & Business Media, 2010.

[10] NREL. "NREL High Performance Computing," http://hpc.nrel.gov/users/systems/peregrine, 2015.

[11] Blender. "Blender – a 3D modelling and rendering package.," http://www.blender.org, 2016.

[12] Ayachit, Utkarsh, *The ParaView Guide: A Parallel Visualization Application*, Kitware, 2015, ISBN 978-1930934306

[13] I. Wald, S. Woop, C. Benthin, G. S. Johnson, and M. Ernst, "Embree – A Kernel Framework for Efficient CPU Ray Tracing," ACM Transactions on Graphics, vol. 14, no. 1, 2014.

[14] P. Cignoni, M. Callieri, M. Corsini, M. Dellepiane, F. Ganovelli, G. Ranzuglia. "MeshLab: an open-source mesh processing tool," *European Italian Conference 2008*, 129-136.

4